# Calcium Niobate Nanosheets Prepared by the Polymerized Complex Method as Catalytic Materials for Photochemical Hydrogen Evolution

Kazuhiko Maeda,[†,‡] Miharu Eguchi,[†] W. Justin Youngblood,[†] and Thomas E. Mallouk*,[†]

[†]*Department of Chemistry, The Pennsylvania State University, University Park, Pennsylvania 16802.*
[‡]*Research fellow of the Japan Society of Promotion Science (JSPS)*

The Dion-Jacobson phase niobate perovskite, $KCa_2Nb_3O_{10}$, was prepared by the polymerized complex (PC) method. The corresponding proton-exchanged material, $HCa_2Nb_3O_{10}$, was then exfoliated by reaction with tetra($n$-butyl)ammonium hydroxide ($TBA^+OH^-$), yielding unilamellar colloidal nanosheets whose lateral dimensions increased with the final calcination temperature in the PC synthesis. By restacking the $TBA^+$-stabilized nanosheets with hydrochloric acid, aggregates of $HCa_2Nb_3O_{10}$ nanosheets were obtained and tested as photocatalytic materials. The rate of $H_2$ production from aqueous methanol solution under band gap irradiation ($\lambda > 300$ nm) was dependent on the calcination temperature. The best materials, prepared by the PC method at the intermediate calcination temperature of 1273 K, had higher activity than those made by a conventional solid state reaction. In contrast, the rate of visible-light hydrogen evolution ($\lambda = 450 \pm 20$ nm) from aqueous ethylenediaminetetraacetic acid (EDTA) solution with materials sensitized by [Ru(bpy)$_2$(4,4'-(PO$_3$H$_2$)$_2$bpy)](PF$_6$)$_2$ (abbreviated RuP$^{2+}$) was essentially insensitive to the preparation conditions. These results suggest that increasing the crystallinity of the nanosheets enhances their activity under band gap irradiation, where catalytic reactions compete with electron−hole recombination within the nanosheet. In contrast, the quantum yield for sensitized $H_2$ production is primarily governed by electron injection efficiency from the excited-state sensitizer into the nanosheet.

## Introduction

Certain layered metal oxides undergo exfoliation upon reaction with organic bases such as tetra ($n$-butyl)ammonium hydroxide, $TBA^+OH^-$, producing unilamellar single-crystalline colloidal sheets (so-called nanosheets).[1−8]

Nanosheets that contain $d^0$ transition-metal cations are typically wide bandgap semiconductors[9] and function as photocatalytic materials.[3,10−15] These semiconducting oxide nanosheets are attractive building blocks for preparing photocatalytic assemblies because of their high surface area and the wide variety of compositions available. The structural flexibility of nanosheets also allows one to construct multicomponent photosystems that incorporate electron donors, acceptors, catalytic nano-particles, or photon antenna molecules.[4,10,11,13,14]

Water splitting into $H_2$ and $O_2$ by illuminated semi-conductor particles has been extensively studied as a

*Corresponding author. Tel: +1-814-863-9637. Fax: +1-814-863-8403. E-mail: tom@chem.psu.edu.

(1) Treacy, M. M. J.; Rice, S. B.; Jacobson, A. J.; Lewandowski, J. T. *Chem. Mater.* **1990,** *2,* 279.
(2) (a) Sasaki, T.; Watanabe, M.; Hashizume, H.; Yamada, H.; Nakazawa, H. *J. Am. Chem. Soc.* **1996,** *118,* 8329. (b) Sasaki, T.; Ebina, Y.; Kitami, Y.; Watanabe, M.; Oikawa, T. *J. Phys. Chem. B* **2001,** *105,* 6116.
(3) (a) Abe, R.; Shinohara, K.; Tanaka, A.; Hara, M.; Kondo, J. N.; Domen, K. *Chem. Mater.* **1997,** *9,* 2179. (b) Abe, R.; Hara, M.; Kondo, J. N.; Domen, K.; Shinohara, K.; Tanaka, A. *Chem. Mater.* **1998,** *10,* 1647.
(4) (a) Keller, S. W.; Kim, H.-N.; Mallouk, T. E. *J. Am. Chem. Soc.* **1994,** *116,* 8817. (b) Keller, S. W.; Johnson, S. A.; Brigham, E. S.; Yonemoto, E. H.; Mallouk, T. E. *J. Am. Chem. Soc.* **1995,** *117,* 12879. (c) Kaschak, M.; Lean, J.; Waraksa, C.; Saupe, G.; Usami, H.; Mallouk, T. E. *J. Am. Chem. Soc.* **1999,** *121,* 3435.
(5) (a) Saupe, G. B.; Waraksa, C. C.; Kim, H.-N.; Han, Y. J.; Kaschak, D. M.; Skinner, D. M.; Mallouk, T. E. *Chem. Mater.* **2000,** *12,* 1556. (b) Kobayashi, Y.; Hata, H.; Salama, M.; Mallouk, T. E. *Nano Lett.* **2007,** *7,* 2142.
(6) Schaak, R. E.; Mallouk, T. E. *Chem. Mater.* **2000,** *12,* 3427.
(7) Han, Y.-S.; Park, I.; Choy, J.-H. *J. Mater. Chem.* **2001,** *11,* 1277.
(8) Schaak, R. E.; Mallouk, T. E. *Chem. Commun.* **2002,** 706.
(9) (a) Sasaki, T.; Watanabe, M. *J. Phys. Chem. B* **1997,** *101,* 10159. (b) Sakai, N.; Ebina, Y.; Takada, K.; Sasaki, T. *J. Am. Chem. Soc.* **2004,** *126,* 5851.
(10) (a) Choy, J.-H.; Lee, H.-C.; Jung, H.; Hwang, S.-J. *J. Mater. Chem.* **2001,** *11,* 2232. (b) Choy, J.-H.; Lee, H.-C.; Jung, H.; Kim, H.; Boo, H. *Chem. Mater.* **2002,** *14,* 2486.
(11) (a) Ebina, Y.; Sasaki, T.; Harada, M.; Watanabe, M. *Chem. Mater.* **2002,** *14,* 4390. (b) Ebina, Y.; Sakai, N.; Sasaki, T. *J. Phys. Chem. B* **2005,** *109,* 17212.
(12) (a) Compton, O. C.; Carroll, E. C.; Kim, J. Y.; Larsen, D. S.; Osterloh, F. E. *J. Phys. Chem. C* **2007,** *111,* 14589. (b) Compton, O. C.; Mullet, C. H.; Chiang, S.; Osterloh, F. E. *J. Phys. Chem. C* **2008,** *112,* 6202. (c) Carroll, E. C.; Compton, O. C.; Madsen, D.; Osterloh, F. E.; Larsen, D. S. *J. Phys. Chem. C* **2008,** *112,* 2394.
(13) (a) Hata, H.; Kobayashi, Y.; Bojan, V.; Youngblood, W. J.; Mallouk, T. E. *Nano Lett.* **2008,** *8,* 794. (b) Ma, R.; Kobayashi, Y.; Youngblood, W. J.; Mallouk, T. E. *J. Mater. Chem.* **2008,** *18,* 5982. (c) Maeda, K.; Mallouk, T. E. *J. Mater. Chem.* **2009,** in press, DOI: 10.1039/b903692j.
(14) (a) Paek, S.-M.; Jung, H.; Lee, Y.-J.; Park, M.; Hwang, S.-J.; Choy, J.-H. *Chem. Mater.* **2006,** *18,* 1134. (b) Kim, T. W.; Hur, S. G.; Hwang, S.-J.; Park, H.; Choi, W.; Choy, J.-H. *Adv. Funct. Mater.* **2007,** *17,* 307.
(15) (a) Maeda, K.; Eguchi, M.; Youngblood, W. J.; Mallouk, T. E. *Chem. Mater.* **2008,** *20,* 6770. (b) Maeda, K.; Eguchi, M.; Lee, S.-H. A.; Youngblood, W. J.; Hata, H.; Mallouk, T. E. *J. Phys. Chem. C* **2009,** *113,* 7962.

potential means of producing clean $H_2$ fuel[16] since photo-assisted water electrolysis was demonstrated by Honda and Fujishima in 1972.[17] With oxide semiconductors under band gap irradiation, electrons and holes are created in the conduction and valence bands, respectively. The particle size of a given photocatalyst affects the number of surface reaction sites. While a smaller particle size increases the density of surface catalytic sites, it means, in principle, a lower degree of crystallinity that can increase the probability of recombination between photogenerated electrons and holes. That is, there is a trade-off between particle size and crystallinity of a given photocatalyst.[18] For example, it has been reported that the photocatalytic activity of certain bulk-type metal oxides for $H_2$ evolution from aqueous solutions containing alcohols as electron donors and for overall water splitting are strongly dependent on the particle size (surface area and crystallinity) of the photocatalysts.[18−21] So far, the size and crystallinity dependence of the photocatalytic activity of oxide nanosheets has yet to be investigated. In this case, the photogenerated carriers move primarily within sheets of ∼1 nm thickness and react with substrates at the surfaces of the sheets. Structural defects can potentially lead to electron−hole recombination in competition with catalytic reactions that may occur on the faces or edges of the sheets.

The polymerized complex (PC) method, originally developed by Pechini,[22] is a powerful and convenient technique that allows for the synthesis of crystalline complex metal oxides even at reduced temperatures.[23−27] This method consists of two essential steps: (1) incorporation of inorganic precursors in a polymer resin with molecular-level dispersion and (2) subsequent calcination to eliminate the polymer and to produce a crystalline metal oxide. The PC method has been applied to the synthesis of a number of layered metal oxides including $Sr_2Nb_x$-$Ta_{2−x}O_7$,[23c] $K_2La_2Ti_3O_{10}$,[24] $KTiNbO_5$,[25] $Ba_5Nb_4O_{15}$,[26] and $KCa_2Nb_3O_{10}$.[27] With this method, the particle size can be controlled by changing the final calcination temperature (step 2).

Recently, we reported mechanistic studies of hydrogen evolution from $HCa_2Nb_3O_{10}$ nanosheets sensitized by ruthenium(II) bipyridyl complexes.[15b] It was also found that $HCa_2Nb_3O_{10}$ nanosheets, which have triple perovskite blocks, show much higher activity for $H_2$ evolution from aqueous 2-propanol solution than do two-layer $HLaNb_2O_7$ perovskite nanosheets.[13c] In this study, the PC method was used to synthesize layered $KCa_2Nb_3O_{10}$, leading to $Ca_2Nb_3O_{10}^-$ nanosheets with a range of lateral dimensions and the corresponding restacked materials as $H_2$-evolving photocatalysts. The rate of photocatalytic $H_2$ evolution was measured using restacked $HCa_2Nb_3O_{10}$ nanosheets, both by UV photolysis from aqueous methanol solution under band gap irradiation ($\lambda > 300$ nm) and by sensitizing the sheets to generate hydrogen from EDTA solutions with visible light ($\lambda = 450 \pm 20$ nm). Factors affecting the activities of the photocatalysts under these conditions are discussed on the basis of physicochemical analyses.

## Experimental Section

**Preparation of $KCa_2Nb_3O_{10}$ by the Polymerized Complex (PC) Method and Subsequent Proton Exchange.** $KCa_2Nb_3O_{10}$ was prepared by the PC method by a variation of the procedure reported by Yamashita et al.[27] In a typical synthesis, 2.905 g of $NbCl_5$ (99.99%, Aldrich) powder was initially dissolved in 100 mL of methanol ($\geq 99.8\%$, Fluka). Then, 0.717 g of $CaCO_3$ (ACS reagent, Aldrich), 0.294 g of KCl (99.0−100.5%, EMD Chemicals), 27 g of ethylene glycol (EG; 100.0%, J.T. Baker), and 21 g of anhydrous citric acid (CA; 99.5%, EMD Chemicals) were added to the solution with stirring. The reaction mixture was heated at ∼373 K to promote complete dissolution on a hot plate stirrer. An excess of KCl (10 mol % of K) was added to the solution to compensate for volatilization of $K_2O$ in the calcination step. The as-obtained transparent solution was heated to 400 K to promote esterification between EG and CA, yielding a glassy resin. The resin was calcined in air at 623−673 K to produce a black powder, which was then subjected to further calcination on an $Al_2O_3$ plate at 923 K for 4 h in air to remove the residual carbon-containing species. Finally, the resulting powder was collected and heated in air at 1173−1473 K for 2 h in an $Al_2O_3$ crucible (ramp rate: 10 $K \cdot min^{-1}$).

Proton-exchange was carried out in aqueous nitric acid (4 M) at room temperature for 3 days with daily centrifugation and replacement of the acid solution.[13a] The product ($HCa_2Nb_3O_{10}$) was isolated by centrifugation, washing, and finally drying at 333 K in an oven overnight.

**Exfoliation and Restacking of $HCa_2Nb_3O_{10}$.** Exfoliation of the as-prepared proton-exchanged materials was performed using aqueous tetra(n-butyl)ammonium hydroxide ($TBA^+OH^-$; Aldrich, 40 wt % in $H_2O$) at room temperature in a similar manner to that reported by Ebina et al.[11] The powder was shaken in an aqueous solution containing $TBA^+OH^-$ for 1 week. The molar ratio of $TBA^+OH^-$ to the exchangeable cations in the layered solids was 1.0. Intercalation of the bulky $TBA^+$ cations results in exfoliation, but some unreacted $HCa_2Nb_3O_{10}$ particles remain. After removing the unreacted $HCa_2Nb_3O_{10}$, the nanosheet colloids were reassembled by adding aqueous hydrochloric acid (HCl; 2.5 M) to form precipitates. The resulting solid was then rinsed several times with pure water to remove residual $TBA^+Cl^-$ and HCl, followed by drying in an oven at 333 K overnight and grinding into a powder using a

(16) (a) Kudo, A.; Kato, H.; Tsuji, I. *Chem. Lett.* **2004**, *33*, 1534. (b) Hoertz, P. G.; Mallouk, T. E. *Inorg. Chem.* **2005**, *44*, 6828. (c) Lee, J. S. *Catal. Surv. Asia* **2005**, *9*, 217. (d) Maeda, K.; Domen, K. *J. Phys. Chem. C* **2007**, *111*, 7851.
(17) Fujishima, A.; Honda, K. *Nature* **1972**, *238*, 37.
(18) Ohtani, B.; Ogawa, Y.; Nishimoto, S. *J. Phys. Chem. B* **1997**, *101*, 3746.
(19) Kudo, A.; Tanaka, A.; Domen, K.; Onishi, T. *J. Catal.* **1988**, *111*, 296.
(20) Sato, J.; Kobayashi, H.; Ikarashi, K.; Saito, N.; Nishiyama, H.; Inoue, Y. *J. Phys. Chem. B* **2004**, *108*, 4369.
(21) Kominami, H.; Murakami, S.; Kato, J.; Kera, Y.; Ohtani, B. *J. Phys. Chem. B* **2002**, *106*, 10501.
(22) Pechini, M. P. U.S. Patent 330697, **1967**.
(23) (a) Kakihana, M. *J. Sol-Gel Sci. Technol.* **1996**, *6*, 7. (b) Kakihana, M.; Yoshimura, M. *Bull. Chem. Soc. Jpn.* **1999**, *72*, 1427. (c) Yoshino, M.; Kakihana, M.; Cho, W. S.; Kato, H.; Kudo, A. *Chem. Mater.* **2002**, *14*, 3369.
(24) Ikeda, S.; Hara, M.; Kondo, J. N.; Domen, K.; Takahashi, H.; Okubo, T.; Kakihana, M. *Chem. Mater.* **1998**, *10*, 72.
(25) Takahashi, H.; Kakihana, M.; Yamashita, Y.; Yoshida, K.; Ikeda, S.; Hara, M.; Domen, K. *J. Alloys Compd.* **1999**, *285*, 77.
(26) Miseki, Y.; Kato, H.; Kudo, A. *Chem. Lett.* **2006**, *35*, 1052.
(27) Yamashita, Y.; Hyuga, K.; Petrykin, V.; Kakihana, M.; Yoshimura, M.; Domen, K.; Kudo, A. *J. Ceram. Soc. Jpn.* **2007**, *115*, 511.

mortar and pestle. The samples thus obtained are designated $HCa_2Nb_3O_{10}$ (*T*), where *T* denotes the final calcination temperature of $KCa_2Nb_3O_{10}$. The band gap of $HCa_2Nb_3O_{10}$ nanosheets is estimated to be approximately 3.50 eV, based on the onset wavelength of the diffuse reflectance spectrum.[13c]

**Modification with Platinum Nanoparticles.** Nanoparticles of platinum (Pt) as a catalyst for $H_2$ evolution were loaded by an in situ photodeposition method[28] onto the external surface of the as-restacked nanosheet materials following the same procedure as described in our previous paper.[15a] The anionic platinum complex $H_2PtCl_6$ was used as the precursor. The loading of Pt was fixed at 0.3 wt % for all samples to eliminate any effects other than those of particle size and crystallinity of the $HCa_2$-$Nb_3O_{10}$ nanosheets.

**Characterization of Materials.** Powder X-ray diffraction (XRD) patterns were obtained with a Philips X'Pert MPD diffractometer using Cu Kα radiation, and transmission electron micrographs (TEM) were obtained using a Jeol JEM-1200EX II microscope. The Brunauer, Emmett, Teller (BET) surface area was measured using a Micromeritics ASAP 2010 instrument at liquid nitrogen temperature. Before nitrogen adsorption isotherms were acquired, the samples were evacuated at 353−363 K for 24 h.
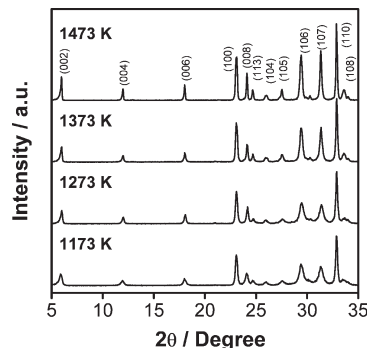
**Steady-State Luminescence Measurements.** Steady-state luminescence spectra were acquired at room temperature in front-face detection mode under 450 nm excitation using a Spex Fluorolog F212 fluorimeter. The composition of the suspension was identical to that used to measure visible-light-sensitized hydrogen production, as will be described below. The scan rate was 1 nm·s$^{-1}$.

**UV Photolysis from Aqueous Methanol Solution.** The reaction was performed by dispersing 5.0 mg of the Pt-loaded sample containing 1 M methanol as an electron donor using a Pyrex reaction cell (10 mL capacity) sealed with a rubber septum. The reactant solution was purged with argon for 5−10 min to remove dissolved air and was then placed in an outer glass jacket where argon gas flowed continuously, to prevent air contamination during the reaction. After that, the reaction vessel was irradiated with a 300 W xenon lamp ($\lambda > 300$ nm). The evolved gases were analyzed by gas chromatography with a thermal conductivity detector and molecular sieve 5A columns at ambient temperature.

**Visible-Light-Sensitized Hydrogen Production.** The reaction was performed in a similar manner to the UV photolysis of methanol but with an aqueous solution containing 0.01 M ethylenediaminetetraacetic acid disodium salt dihydrate (EDTA; 99.95%, Aldrich) as an electron donor and 20 μM [Ru-(bpy)$_2$(4,4'-(PO$_3$H$_2$)$_2$bpy)](PF$_6$)$_2$ (RuP$^{2+}$) as a photosensitizer. RuP$^{2+}$ was synthesized by the method of Schmehl et al.[29] Visible light irradiation was performed using a 300 W xenon lamp fitted with a band-pass filter ($\lambda = 450 \pm 20$ nm).

## Results and Discussion

**Characterization.** Figure 1 shows powder X-ray diffraction (XRD) patterns of as-prepared $KCa_2Nb_3O_{10}$ samples with different final calcination temperatures. All samples show single phase diffraction patterns assigned to layered $KCa_2Nb_3O_{10}$.[30] The diffraction peaks



**Figure 1.** XRD patterns of layered $KCa_2Nb_3O_{10}$ samples prepared by the PC method at different calcination temperatures.

of $KCa_2Nb_3O_{10}$ became stronger and narrower as the calcination temperature was increased from 1173 to 1473 K, indicating increasing crystallinity at more elevated calcination temperatures. This behavior is typical of PC-derived metal oxides calcined at different temperatures[23,24] and is consistent with the previous report by Yamashita et al. for $KCa_2Nb_3O_{10}$.[27] It should be noted that the diffraction peaks become narrower not only for (00*l*) ($l \geq 2$) reflections that correspond to ordering along the stacking axis but also for (*hk*0) reflections (100) and (110) corresponding to in-plane lattice directions (i.e., (100) and (110)) and for several (*hkl*) reflections. This indicates that size of the scattering domains increases not only in the stacking direction but in the in-plane directions as well. The same tendency was observed in XRD patterns of proton-exchanged samples, $HCa_2$-$Nb_3O_{10}$ (see Supporting Information, Figure S1).

The $HCa_2Nb_3O_{10}$ samples thus obtained were then exfoliated by reaction with TBA$^+$OH$^-$. Figure 2 shows TEM images of exfoliated TBA$_x$H$_{1-x}$Ca$_2$Nb$_3$O$_{10}$ nanosheets[31] derived from $KCa_2Nb_3O_{10}$ powders that were calcined at different temperatures. The lateral dimensions of the $HCa_2Nb_3O_{10}$ (1173 K) nanosheets range from 100 to 700 nm, which is obviously smaller than that reported for the same material made by the solid state reaction (SSR) of the binary oxides and carbonates (typically, a few micrometers).[12] The lateral dimensions of the PC-derived nanosheets tend to increase with increasing $KCa_2Nb_3O_{10}$ calcination temperature, although some fragmented sheets with lateral dimensions less than 100 nm are evident even at higher temperatures. The trend of increasing particle size is the same as that suggested by the XRD patterns (Figure 1 and Supporting Information Figure S1), although it should be noted that the diffraction linewidths are dominated by the smallest particles in the distribution and linewidths from crystalline domains larger than ~100 nm are determined by
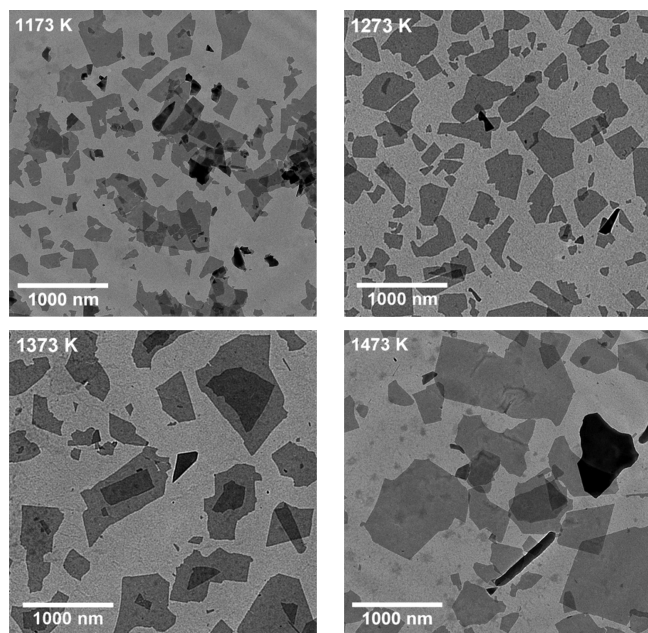
(28) Kraeutler, B.; Bard, A. J. *J. Am. Chem. Soc.* **1978**, *100*, 4317.
(29) Montalti, M.; Wadhwa, S.; Kim, W. Y.; Kipp, R. A.; Schmehl, R. H. *Inorg. Chem.* **2000**, *39*, 76.
(30) Jacobson, A. J.; Johnson, J. W.; Lewandowski, J. T. *Inorg. Chem.* **1985**, *24*, 3727.
(31) The formula TBA$_x$H$_{1-x}$Ca$_2$Nb$_3$O$_{10}$ is used to describe HCa$_2$N-b$_3$O$_{10}$ nanosheets exfoliated by reaction with excess TBA$^+$OH$^-$. The value of *x* has not been quantified, although previous studies with layered oxides and phosphates of similar charge density have shown that the exfoliated sheets have *x* ≈ 0.4: (a) Fang, M.; Kim, C. H.; Saupe, G. B.; Kim, H.-H.; Waraksa, C. C.; Miwa, T.; Fujishima, A.; Mallouk, T. E. *Chem. Mater.* **1999**, *11*, 1526. (b) Kaschak, D. M.; Johnson, S. A.; Hooks, D.; Kim, H.-N.; Ward, M. D.; Mallouk, T. E. *J. Am. Chem. Soc.* **1998**, *120*, 10887.
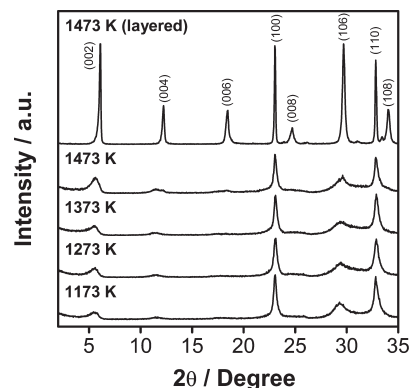
**Figure 2.** TEM images of exfoliated $TBA_xH_{1-x}Ca_2Nb_3O_{10}$ derived from layered $KCa_2Nb_3O_{10}$ calcined at different temperatures.



**Figure 3.** XRD patterns of restacked $HCa_2Nb_3O_{10}$ nanosheets derived from layered $KCa_2Nb_3O_{10}$ calcined at different temperatures. Data for layered $HCa_2Nb_3O_{10}$ (1473 K) are also given for comparison.

instrumental factors. The TEM images show clearly that the lateral dimensions of $Ca_2Nb_3O_{10}{}^-$ nanosheets can be controlled by applying the PC method to the synthesis of the parent $KCa_2Nb_3O_{10}$ powder, followed by ion exchange and exfoliation.

The colloidal nanosheets were precipitated by adding HCl to form restacked $HCa_2Nb_3O_{10}$ materials for photocatalysis experiments. Figure 3 shows XRD patterns of restacked $HCa_2Nb_3O_{10}$ nanosheets, along with the data for layered $HCa_2Nb_3O_{10}$ made by acid exchange of $KCa_2Nb_3O_{10}$ (1473 K) for comparison. The XRD patterns of the restacked nanosheets exhibit broad and weaker (001) diffraction peaks, which are shifted to lower angle than the corresponding (002) peak in layered $HCa_2Nb_3O_{10}$ owing to turbostratic ordering and increased hydration. A significant reduction of intensity of the (00*l*) ($l \geq 2$) peaks relative to the parent solids is observed, indicating a much less ordered lamellar structure in the restacked materials. Strong (100) and (110) diffraction peaks corresponding to in-plane lattice directions are preserved but broadened. The (*hkl*) reflections are weak and more substantially broadened. This indicates that the in-plane crystallinity of the $Ca_2Nb_3O_{10}{}^-$ sheets is preserved after the exfoliation–reassembling procedure but that there is relatively poor registry between sheets. Unlike the corresponding layered $KCa_2Nb_3O_{10}$ and $HCa_2Nb_3O_{10}$ samples, however, no successive change with respect to calcination temperature could be identified. The line width of the (*hk*0) reflections, corresponding to a scattering domain size of 20–30 nm, most likely reflects the bending of the flexible nanosheets[32] in the restacked materials rather than a decrease in the lateral dimensions of the sheets, which are always

much larger than 20–30 nm. The specific surface area of the restacked nanosheets decreased with increasing calcination temperature, as shown in Table 1. This trend is consistent with the increase in the lateral dimensions of the nanosheets with increasing calcination temperature (Figure 2).

**Photocatalytic Activity of Restacked $HCa_2Nb_3O_{10}$ Nanosheets.** Figure 4 (solid circles) shows the rate of $H_2$ evolution from aqueous methanol solution catalyzed by Pt-loaded, restacked $HCa_2Nb_3O_{10}$ nanosheets under band gap irradiation ($\lambda > 300$ nm) as a function of the calcination temperature of $KCa_2Nb_3O_{10}$. The reaction scheme is illustrated in Scheme 1A. All samples showed reasonable activity, and no reaction took place in the dark. After 2–3 h of irradiation, the number of moles of $H_2$ evolved surpassed that of the catalysts employed (ca. 9–10 $\mu$mol), indicating that the reactions take place photocatalytically. Interestingly, these photocatalysts show a volcano pattern in hydrogen evolution rate versus calcination temperature, with a maximum in activity at 1273 K.

We recently reported that restacked $HCa_2Nb_3O_{10}$ nanosheets mediate electron transport between the surface bound $RuP^{2+}$ sensitizer and catalytic Pt nanoparticles, leading to efficient visible light $H_2$ evolution in the presence of EDTA as a sacrificial electron donor.[15b] Scheme 1B shows the reaction scheme. Figure 4 (open diamonds) also shows the effect of the calcination temperature of $KCa_2Nb_3O_{10}$ on the activity of sensitized $H_2$ evolution by Pt-loaded restacked $HCa_2Nb_3O_{10}$ nanosheets under visible light irradiation ($\lambda = 450 \pm 20$ nm). Although the excited-state of $RuP^{2+}$ ($^*RuP^{2+}$) has a sufficiently negative redox potential ($RuP^{3+}/^*RuP^{2+} = -0.95$ V vs NHE),[33] no $H_2$ production takes place unless a suitable electron transport material is present,[34] as confirmed by a control experiment carried out in the absence of Pt-loaded nanosheets. In contrast to the reaction with methanol under band gap irradiation, the visible-light photocatalytic activity is essentially constant, regardless of the calcination temperature.
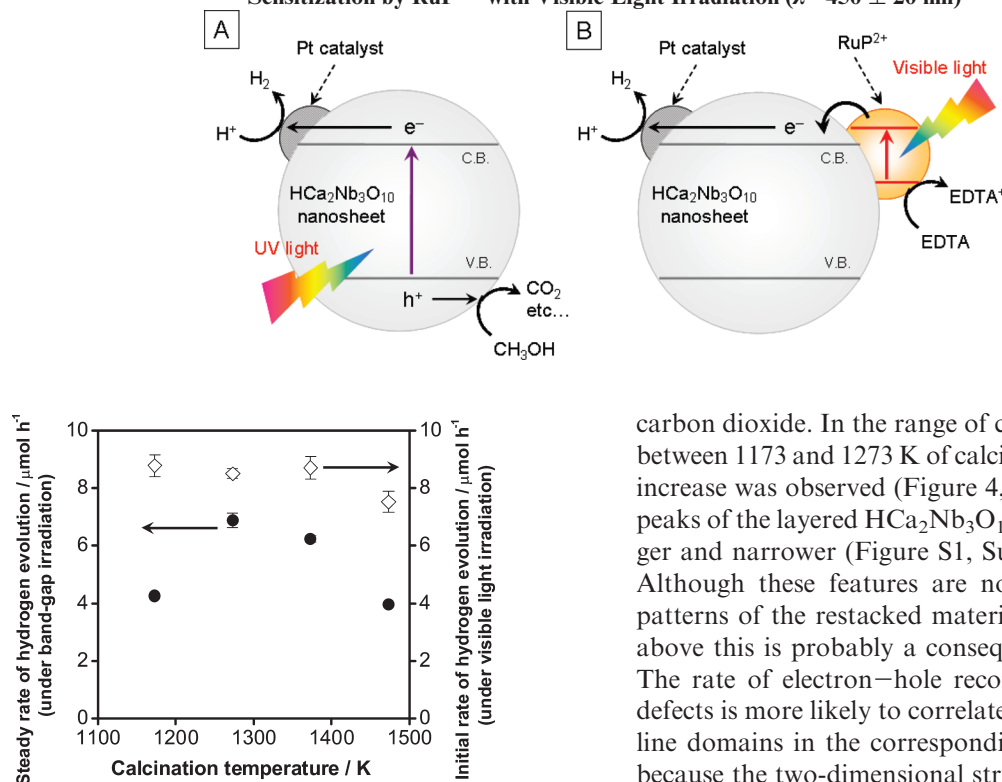
(32) Solin, S. A.; Hines, D.; Jacobson, A. J.; Mahanti, S. D. *Solid State Commun.* **1996**, *100*, 143.

(33) Park, H.; Bae, E.; Lee, J.-J.; Park, J.; Choi, W. *J. Phys. Chem. B* **2006**, *110*, 8740.

**Table 1. Specific Surface Area, Photocatalytic Hydrogen Evolution Rate, and MLCT Quenching Efficiency of Restacked HCa$_2$Nb$_3$O$_{10}$ Nanosheets Prepared under Different Conditions**

| | calcination condition | | | rate of H$_2$ evolution,[a] $\mu$mol·h$^{-1}$ | | |
|---|---|---|---|---|---|---|
| entry | temp, K | time, h | specific surface area, m$^2$·g$^{-1}$ | UV photolysis[b] | RuP$^{2+}$-sensitized[c] | quenching efficiency,[d] % |
| 1 | 1173 | 2 | 72−73 | 4.3 | 8.8 ± 0.4 | 76 |
| 2 | 1273 | 2 | 58−59 | 7.1 | 8.5 ± 0.2 | 77 |
| 3 | 1373 | 2 | 53−54 | 6.0 | 8.7 ± 0.4 | 73 |
| 4 | 1473 | 2 | 42−43 | 3.9 | 7.5 ± 0.4 | 71 |
| 5[e] | 1473 | 10 | 50−51 | 4.4 | 8.4 ± 0.4 | 64 |

[a] Reaction conditions: catalyst, 5.0 mg (0.3 wt % Pt-loaded); reaction solution, aqueous solution (2.0 mL). [b] Steady rate of H$_2$ evolution from 10 vol % methanol solution; irradiation wavelength, $\lambda > 300$ nm. [c] Initial rate of H$_2$ evolution from 0.01 M EDTA solution; irradiation wavelength, $\lambda = 450 \pm 20$ nm. [d] Estimated on the basis of the ratio of the luminescence intensity to the RuP$^{2+}$-only case. [e] Prepared by a conventional solid state reaction (see also ref 37).

**Scheme 1. Schematic Illustration of H$_2$ Production Based on (A) Band-Gap Excitation under UV Irradiation ($\lambda > 300$ nm) and (B) Sensitization by RuP$^{2+}$ with Visible Light Irradiation ($\lambda = 450 \pm 20$ nm)**





**Figure 4.** Dependence of the rate of H$_2$ evolution from 0.3 wt % Pt-loaded restacked HCa$_2$Nb$_3$O$_{10}$ nanosheets under band gap ($\lambda > 300$ nm) and visible light irradiation ($\lambda = 450 \pm 20$ nm) on the calcination temperature of KCa$_2$Nb$_3$O$_{10}$. Reaction conditions under band gap irradiation: catalyst, 5.0 mg; aqueous methanol solution (1 M, 2.0 mL); light source, xenon lamp (300 W). Reaction conditions under visible light irradiation: catalyst, 5.0 mg; aqueous solution containing 0.01 M EDTA and 20 $\mu$M RuP$^{2+}$ (2.0 mL); light source, xenon lamp (300 W) with a band-pass filter.

**Factors Affecting Photochemical Hydrogen Evolution Yields.** In H$_2$ evolution from aqueous methanol solution under band gap irradiation ($\lambda > 300$ nm), the restacked HCa$_2$Nb$_3$O$_{10}$ nanosheets undergo photoexcitation, producing electrons and holes in the conduction and valence bands, respectively (Scheme 1A). The photogenerated carriers have to migrate in the two-dimensional Ca$_2$Nb$_3$O$_{10}$$^-$ sheets without recombination to carry out redox reactions. Conduction band electrons react with H$^+$ at the Pt nanoparticles to form H$_2$, while holes in the valence band are consumed by oxidation of methanol to give

carbon dioxide. In the range of calcination temperatures between 1173 and 1273 K of calcination where an activity increase was observed (Figure 4, solid circles), the XRD peaks of the layered HCa$_2$Nb$_3$O$_{10}$ samples became stronger and narrower (Figure S1, Supporting Information). Although these features are not evident in the XRD patterns of the restacked materials (Figure 3), as noted above this is probably a consequence of layer bending. The rate of electron−hole recombination at structural defects is more likely to correlate with the size of crystalline domains in the corresponding layered compounds, because the two-dimensional structure is preserved even after exfoliation and restacking. The initial increase in activity with calcination temperature is therefore probably a consequence of the improved crystallinity of HCa$_2$Nb$_3$O$_{10}$ nanosheets. It is known that metal-oxides with poorer crystallinity (e.g., samples calcined at lower temperatures) contain structural imperfections, which contribute directly to a decrease in photocatalytic activity.[18−21,23c,24] Ohtani et al. recently reported by means of action spectrum analysis and time-resolved infrared absorption spectroscopy that crystallization indeed increases the lifetime of photoexcited carriers, resulting in the enhancement of photocatalytic activity.[35] Calcination at temperatures higher than 1273 K, on the other hand, resulted in decreasing activity, which may be attributable to a loss of specific surface area accompanied by an increase in the lateral dimensions of the nanosheets, as
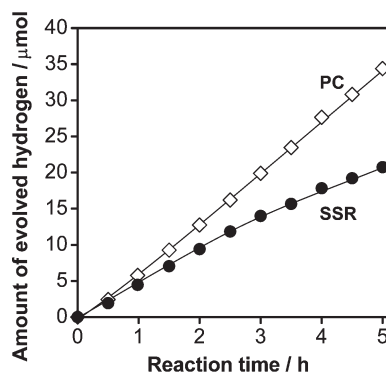
(34) Kalyanasundaram, K. *Coord. Chem. Rev.* **1982**, *46*, 159.
(35) Amano, F.; Yamakata, A.; Nogami, K.; Osawa, M.; Ohtani, B. *J. Am. Chem. Soc.* **2008**, *130*, 17650.

indicated by TEM images (Figure 2). As shown in Table 1, the specific surface area of the restacked nanosheets did decrease with increasing calcination temperature. Many conventional metal oxide photocatalysts have been reported to exhibit a decrease in activity with decreasing specific surface area.[20,21,23c,24] This is caused by a decrease in the number of reaction sites on the catalyst surface and/or the coverage of the surface with excess amounts of catalytic metals.

In the case of sensitized $H_2$ evolution with visible light ($\lambda = 450 \pm 20$ nm), the reaction rate was almost the same, regardless of the calcination temperature (Figure 4, open diamonds), meaning that structural properties of the nanosheet samples have little effect on the overall quantum efficiency under these conditions. As shown in Scheme 1B, sensitized $H_2$ evolution occurs when electrons injected by excited-state $RuP^{2+}$ are consumed by reduction of $H^+$ at the surface of the Pt nanoparticle catalysts. We recently determined that the quantum efficiency of hydrogen evolution in this system is determined by the quantum efficiency of charge injection, since electron transport within the sheet is substantially faster than charge recombination or reaction of $EDTA^{2-}$ with $RuP^{3+}$.[15b] To confirm this conclusion with materials prepared by the PC method, the efficiency of electron injection from photoexcited $RuP^{2+}$ into the conduction band of restacked nanosheets was investigated by means of steady-state luminescence spectroscopy. In solution, $RuP^{2+}$ has a luminescence peak at ~650 nm corresponding to emission from the metal-to-ligand charge transfer (MLCT) state.[29] The luminescence intensity decreased upon addition of restacked $HCa_2Nb_3O_{10}$ nanosheets to the sensitizer solution in each case, indicating electron injection from photoexcited $RuP^{2+}$ into the conduction band of nanosheets.[36] Consistent with the trend shown in Figure 4 (open diamonds), there was no significant change in quenching efficiency with increasing calcination temperature (see Supporting Information, Figure S2). As expected the efficiency of the electron injection is insensitive to the crystallinity of the restacked $HCa_2$-$Nb_3O_{10}$ nanosheets, and the efficiency of sensitized $H_2$ production is governed by the electron injection efficiency, consistent with our previous observations.[15b] Although structural imperfections in the nanosheets may affect the rate of electron transport to the Pt nanoparticles, this process is still apparently quite fast relative to charge recombination.

**Comparison with Photocatalysts Prepared by the Solid State Reaction Method.** Although there was almost no difference in activity for sensitized $H_2$ production between catalysts prepared by the PC and SSR methods (Table 1), the activity under band gap irradiation varied significantly. Figure 5 shows time courses of UV-light-driven $H_2$ evolution from aqueous methanol solutions by



**Figure 5.** Time courses of $H_2$ evolution from Pt-loaded restacked $HCa_2Nb_3O_{10}$ nanosheets prepared by the PC method (calcination at 1273 K for 2 h) and solid state reaction under band gap irradiation ($\lambda >$ 300 nm). Reaction conditions: catalyst, 5.0 mg; aqueous methanol solution (1 M, 2.0 mL); light source, xenon lamp (300 W).

Pt-loaded restacked $HCa_2Nb_3O_{10}$ nanosheets that were prepared by the PC and SSR methods.[37] The activity of the PC catalyst (7.1 $\mu$mol·h$^{-1}$) was 1.6 times higher than that of the SSR catalyst (4.4 $\mu$mol·h$^{-1}$). It is notable that the PC-derived catalyst calcined at 1373 K also showed higher activity (Table 1), even though this material has a surface area (53–54 m$^2$·g$^{-1}$) similar to that of the SSR catalyst (50–51 m$^2$·g$^{-1}$). Therefore, the improved activity of the PC catalysts cannot be explained simply in terms of the larger specific surface area. It has been proposed that SSR involves localized segregation of constituent elements in the final product, generating structural defects during the synthesis.[23a] Such structural imperfections may contribute directly to a decrease in photocatalytic activity, because they act as recombination centers for photogenerated electrons and holes. Domen et al. have reported that $NiO_x$-loaded lamellar $K_2La_2Ti_3O_{10}$ prepared by the PC method shows higher activity for overall water splitting than that obtained by the SSR method, even though each sample had almost the same specific surface area.[24] They suggest that the less defective nature of the PC sample leads to the higher activity. Accordingly, it is likely that $HCa_2Nb_3O_{10}$ nanosheets prepared by the PC method have lower defect density than the SSR sample, resulting in a higher rate of $H_2$ evolution.

It should also be noted that layered $KCa_2Nb_3O_{10}$ cannot be prepared by the SSR method with calcination at 1273 K for 2 h, whereas the PC method results in phase-pure $KCa_2Nb_3O_{10}$, even at lower temperatures (Figure 1). XRD analysis showed that the SSR product obtained at 1273 K contained small amounts of crystalline impurity phases ($K_4Nb_6O_{17}$, $Ca_{2.67}Nb_{1.33}O_6$, $Ca_2Nb_2O_7$, and $CaNb_2O_6$) in addition to $KCa_2Nb_3O_{10}$ (see Supporting Information, Figure S3). Thus, it can be concluded that the PC

(36) Scattering by the suspended particles is likely to affect the apparent luminescence efficiency. Because the scattering is a function of particle size and composition, it is reasonable to assume that scattering causes deviations in the quenching efficiency among the different samples to some extent.

(37) $KCa_2Nb_3O_{10}$ was prepared by heating a mixture of $K_2CO_3$ (99.9%, J. T. Baker), $CaCO_3$ (ACS reagent, Aldrich), and $Nb_2O_5$ (99.99%, Aldrich) powders (K/Ca/Nb = 1.1/2/3 by mole) at 1473 K for 10 h in air (ramp rate: 10 K·min$^{-1}$) according to previous literature reports (refs 13a, 14b, and 31). To prepare restacked nanosheets, the as-synthesized $KCa_2Nb_3O_{10}$ was subjected to proton-exchange, followed by exfoliation-restacking as described in the Experimental Section.

method allows one in this case to achieve greater crystallinity at lower temperatures and with shorter reaction times. Our preliminary investigations have shown that the PC method can be applied to other nanosheet photocatalysts such as $HSr_2Nb_3O_{10}$, and in this case enhanced photocatalytic activity was also obtained (see Supporting Information, Figure S4). As semiconductor nanosheets are useful components of various kinds of photocatalytic reaction systems,[10−14] these results suggest the possibility of improving those systems by optimizing the preparation conditions of the nanosheets via the PC method.

## Conclusions

Platinized restacked $HCa_2Nb_3O_{10}$ nanosheets function both as photocatalysts for $H_2$ evolution from aqueous methanol solutions under band gap irradiation ($\lambda > 300$ nm) and as building blocks for $RuP^{2+}$-sensitized $H_2$ evolution from aqueous EDTA solutions with visible light ($\lambda = 450 \pm 20$ nm). Reducing structural imperfections and increasing the specific surface area of the nanosheets both contribute to enhancing the activity under band gap irradiation. In contrast, the rate of sensitized $H_2$ production is not signficantly affected by these structural properties. This study also suggests that it is possible to improve photocatalytic activity of other nanosheets by refining the preparation condition of the parent layered solids.

**Supporting Information Available:** XRD patterns of proton-exchanged $KCa_2Nb_3O_{10}$ samples (Figure S1), luminescence spectra for Pt-loaded restacked $HCa_2Nb_3O_{10}$ nanosheets sensitized by $RuP^{2+}$ with 450 nm excitation (Figure S2), XRD patterns of layered $KCa_2Nb_3O_{10}$ samples prepared by solid state reactions under different conditions (Figure S3), and time courses of $H_2$ evolution from Pt-loaded restacked $HSr_2Nb_3O_{10}$ nanosheets prepared via the PC and SSR methods under UV irradiation (Figure S4) (PDF). This material is available free of charge via the Internet at http://pubs.acs.org.